Flow field and bipolar plate design for AEM electrolyzer

Vladimir L. Meca [a], Laura Quiroga-Nicolas [b], Rafael d'Amore-Domenech [c], Óscar Santiago [d], Antonio Villalba-Herreros [e], Teresa J. Leo [f]

[a] Universidad Politécnica de Madrid, Madrid, Spain, vl.meca@upm.es, CA
[b] Universidad Politécnica de Madrid, Madrid, Spain, laura.quiroga@alumnos.upm.es,
[c] Universidad Politécnica de Madrid, Madrid, Spain, r.damore@upm.es,
[d] University of Bremen, Bremen, Germany, santiago@uni-bremen.de,
[e] Universidad Politécnica de Madrid, Madrid, Spain, antonio.villalba@upm.es,
[f] Universidad Politécnica de Madrid, Madrid, Spain, teresa.leo.mena@upm.es

Abstract:

Anion exchange membrane (AEM) electrolyzers have attracted interest for hydrogen production due to their potential to combine the use of non-noble catalysts with moderate operating conditions and reduced system cost. These characteristics make AEM technology particularly appealing for decentralized and maritime applications. However, current AEM electrolyzers face significant drawbacks at cell level, including limited durability, leakage issues, poor reproducibility of cell assemblies, and a lack of standardized design methodologies for bipolar plates and flow fields. These limitations hinder performance assessment and technology scaling. This work addresses these challenges by presenting a process for design, manufacturing, and experimental validation of bipolar plates and flow fields for AEM electrolyzer single cells. The study focuses on development of additively manufactured plates, enabling rapid iteration of flow field geometries and sealing concepts while targeting mass and cost reduction. Particular attention is devoted to plate design aspects important for AEM operation, including leak-tight sealing strategies, control of compression and torque during assembly, and mechanical stability under operating pressure. To support this development, a dedicated experimental test bench for AEM single cells has been designed and constructed. The test bench allows control of assembly torque, operating conditions, and fluid management, enabling reproducible testing and comparison between different plate designs and materials. The setup is conceived to isolate the influence of flow field architecture and plate design on electrochemical performance and operational robustness. The proposed approach provides a framework to overcome key AEM electrolyzer drawbacks related to cell assembly and component integration. The final objective is the fabrication and testing of a functional AEM electrolyzer single cell incorporating components (membrane, electrodes, gaskets and plates) developed within the Solener-CM project consortium. By focusing on methodology rather than on single optimized design, this work contributes to improve reliability, scalability, and techno-economic potential of AEM electrolyzers for maritime hydrogen production.

Keywords:

AEM, anion exchange membrane electrolyzer; bipolar plates; coating; sputtering.

1. Introduction

Hydrogen production via water electrolysis is gaining increasing attention as a key pathway toward sustainable energy systems. Among the different electrolysis technologies, anion exchange membrane (AEM) electrolyzers have emerged as a promising alternative due to their potential to combine the advantages of alkaline and proton exchange membrane systems. Despite this potential, several challenges remain at the cell level, where the design of critical components such as bipolar plates and flow fields plays a decisive role in determining overall performance and efficiency.

In this context, this section provides an overview of the state of the art, including a comparison of the main electrolysis technologies, a description of AEM cell architecture and components, the specific limitations associated with this technology, and a review of the most relevant flow field designs and additive manufacturing approaches for bipolar plates.

1.1. Context and motivation: hydrogen production and AEM electrolyzers

Actions to mitigate climate change and achieve an immediate reduction in greenhouse gas (GHG) emissions are central objectives of the Paris Agreement, which aims to limit global warming to below 1.5 °C in the coming decades [1]. At the same time, continuous population growth is driving a steady increase in global energy demand. However, this demand is still predominantly met by fossil fuels, which remain the primary source of pollutant emissions responsible for global warming [2]. In response to this challenge, there is a growing interest in clean energy technologies capable of decoupling energy production from environmental impact. Renewable energy sources such as wind, hydropower, and solar provide sustainable alternatives; nevertheless, their inherent intermittency introduces significant challenges for energy supply reliability [1]. Within this context, hydrogen has emerged as a promising energy carrier, particularly due to its capability to act as an energy storage medium [3,4]. Its versatility allows energy conversion either through direct combustion or via electrochemical systems for electricity generation [1,3]. Green hydrogen, produced through water electrolysis powered by renewable energy, is therefore considered a key pathway toward a sustainable energy future. Despite its potential, electrolysis currently accounts for less than 0.1 % of global hydrogen production, while approximately 65 % is still generated from fossil-based (gray) processes [4]. Water electrolysis can be performed using several technologies at different stages of maturity, including anion exchange membrane electrolysis (AEM), proton exchange membrane electrolysis (PEM), conventional alkaline water electrolysis (AWE), and solid oxide electrolysis (SOE) [5]. These technologies are generally classified into low-temperature and high-temperature systems based on their operating conditions [6]. The electrolysis process involves the splitting of water into hydrogen (H_2) and oxygen (O_2) through the application of electrical energy. The overall reaction and its corresponding standard potential are given by [4,7]:

$$2H_2O(l) \rightarrow 2H_2(g) + O_2(g), \quad Eo = 1.23\ V \qquad \text{(R1)}$$

Among these technologies, anion exchange membrane electrolysis (AEM) has recently gained significant attention as a promising alternative, although it remains at an early stage of development with limited commercial deployment. This technology combines key advantages of alkaline and PEM systems [8].

Table 1. *Comparison of operating parameters between alkaline (ALK) and anion exchange membrane (AEM) electrolyzers.*

Parameter	ALK	AEM
Anode reaction	$2OH^- \rightarrow H_2O + ½O_2 + 2e^-$	$2OH^- \rightarrow H_2O + ½O_2 + 2e^-$
Cathode reaction	$2H_2O + 2e^- \rightarrow H_2 + 2OH^-$	$2H_2O + 2e^- \rightarrow H_2 + 2OH^-$
Overall cell	$H_2O \rightarrow H_2 + ½O_2$	$H_2O \rightarrow H_2 + ½O_2$
Electrolyte	KOH/NaOH	KOH/NaOH
Membrane	Asbestos/ Zirfon /Ni	Fumatech
Electrode/catalyst	Nickel coated perforated stainless steel	Nickel
Electrode/catalyst	Nickel coated perforated stainless steel	Nickel or NiFeCo alloys
Gas diffusion layer	Nickel mesh	Nickel foam /carbon cloth
Bipolar plates	Stainless Steel /Nickel coated stainless steel	Stainless Steel /Nickel coated stainless steel
Normal current density	0.2 – 0.8 A/cm^2	0.2 – 2 A/cm^2
Voltage range (limits)	1.4 – 3 V	1.4 – 2.0 V
Operating temperature	70 – 90	40-60
Cell pressure	<30 bar	<35 bar
H2 purity	99.05 % - 99.99998 %	99.9 % - 99.9999 %
Efficiency	50 %-78 %	57 %-59 %
Lifetime (stack)	60000 h	>30000 h
Development status	mature	R&D
Electrode area	10000-30000 cm^2	<300 cm^2

On the one hand, the alkaline environment enables the use of non-noble catalysts, reducing material costs and avoiding the need for platinum group metals (PGMs) [5,9]. On the other hand, the use of a solid polymer membrane, similar to PEM systems, allows operation at higher current densities compared to conventional alkaline electrolysis [10]. Tables 1 and 2 summarize the main characteristics and operating parameters of the most relevant water electrolysis technologies.

Table 2. *Comparison of proton exchange membrane (PEM) and solid oxide electrolyzer (SOE) technologies.*

Parameter	PEM	SOE
Anode reaction	$H_2O \rightarrow 2H^+ + ½O_2 + 2e^-$	$O^{2-} \rightarrow ½O_2 + 2e^-$
Cathode reaction	$2H^+ + 2e^- \rightarrow H_2$	$H_2O + 2e^- \rightarrow H_2 + O^{2-}$
Overall cell	$2H_2O \rightarrow H_2 + ½O_2$	$H_2O \rightarrow H_2 + ½O_2$
Electrolyte	Solid polymer electrolyte (PFSA)	Yttia stabilized Zirconia (YSZ)
Membrane	Nafion®	Solid electrolyte YSZ
Electrode/catalyst	Iridium oxide	Ni/YSZ
Electrode/catalyst	Platinum carbon	Perovskites (LSCF, LSM) (La, Sr, Co, FE) (La, Sr,Mn)
Gas diffusion layer	Titanium mesh /carbon cloth	Nickel mesh /foam
Bipolar plates	Platinum /Gold-coated Titanium or Titanium	Cobalt coated stainless steel
Normal current density	1 – 2 A/cm^2	0.3 – 1 A/cm^2
Voltage range (limits)	1.4 – 2.5 V	1.0 – 1.5 V
Operating temperature	50-80	700-850
Cell pressure	<70 bar	1 bar
H2 purity	99.9 % - 99.9999 %	99.9 %
Efficiency	50 % - 83 %	89 % (laboratory)
Lifetime (stack)	50000-80000 h	20000 h
Development status	Commercialized	R&D
Electrode area	1500 cm^2	200 cm^2

Anion exchange membrane electrolyzers employ a solid polymer membrane capable of transporting hydroxyl ions (OH^-), which fulfills a dual function: acting as an electrolyte while physically separating the anode and cathode compartments [11]. Upon application of electrical energy, water splitting occurs through two fundamental electrochemical reactions: the oxygen evolution reaction (OER) at the anode and the hydrogen evolution reaction (HER) at the cathode. Hydroxyl ions migrate through the membrane from the cathode to the anode, while electrons flow through the external circuit, maintaining charge balance and enabling continuous operation [4,8].

1.2. Single-cell architectures in AEM electrolyzers

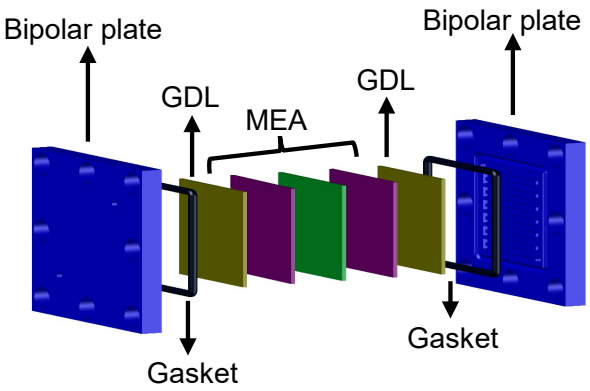

Figure 1. *Schematic representation of the main components of an alkaline exchange membrane electrolyzer.*

AEM electrolyzers are composed of multiple layers assembled into a compact electrochemical cell architecture. This layered structure includes bipolar plates, gas diffusion layers (GDLs), catalyst layers (CLs), and a solid anion exchange membrane [8]. At the core of the system lies the membrane electrode assembly (MEA), which integrates the membrane, catalyst layers, and gas diffusion layers. The MEA is the functional heart of the electrolyzer, where the electrochemical reactions take place and ionic transport is enabled. Structurally, the MEA is arranged in a sandwich configuration between two plates—referred to as monopolar plates in single cell configurations and bipolar plates in stack systems. In stack configurations, these plates additionally act as separators between adjacent cells, ensuring electrical continuity and fluid isolation [12]. Table 3 summarizes the main components of an AEM electrolyzer and their respective functions.

Table 3. *Main components of an alkaline exchange membrane electrolyzer and their principal functions.*

Component	Principal Function
Bipolar plates	Distribute the electrical current, reactants, and separate the gases produced at the anode and cathode [13].
Gasket	Ensure good mechanical contact and avoid leaks.
GDL	Transfer the products generated at the catalyst layers and distribute the reactants [13].
MEA	Conducts ions and separates anode and cathode sides [14].

Despite their potential, anion exchange water electrolyzers (AEM) still face significant challenges at the single-cell level, particularly in terms of durability, mechanical robustness, and long-term stability. These limitations are primarily associated with the need to develop low-cost materials capable of operating under highly alkaline conditions (pH > 13) while maintaining adequate electrical conductivity and chemical stability over extended operation times [14,15]. Compared to more mature electrolysis technologies, AEM systems exhibit relatively short lifetimes, typically below 2000 h [16,17], which remains a major barrier to commercialization.

To address these issues, significant research efforts have focused on the development of non-noble metal electrocatalysts for both the oxygen evolution reaction (OER) and hydrogen evolution reaction (HER). One of the key advantages of the alkaline environment is the possibility of using platinum group metal (PGM)-free catalysts, thereby reducing system cost [17]. In contrast, acidic systems require the use of noble metals such as iridium and platinum due to their superior stability [16]. However, even under alkaline conditions, non-noble materials are still susceptible to degradation, leading to insufficient long-term performance. In parallel, advances in anion exchange membranes have led to the development of commercially available materials with improved ionic conductivity and chemical stability. Examples include Sustainion® X37-50 and Fumasep FAA-3-50 membranes, which exhibit high hydroxide conductivity and enhanced durability in alkaline environments [18]. Nevertheless, further improvements are still required to mitigate degradation mechanisms and extend operational lifetimes.

1.3. Bipolar plates and flow field designs in water electrolyzers

As illustrated in Figure 1, bipolar plates are critical components in electrochemical cells, representing a significant fraction of both the total system volume and cost [19]. In single-cell configurations, monopolar plates are typically used, whereas bipolar plates are employed in stack systems, where they simultaneously act as current collectors and separators between adjacent cells [19]. Bipolar plates fulfill several essential functions. They distribute reactants through the flow channels to the electrodes, ensure uniform reactant coverage across the active area, and enable the removal of gaseous products generated during operation. Additionally, they act as physical barriers that prevent mixing between anodic and cathodic streams, which is crucial for both safety and efficiency [20,21]. Since flow channels are integrated into the surface of the bipolar plates, their design plays a key role in determining fluid distribution, pressure drop, and gas removal [22]. Three main flow field configurations are commonly reported in the literature among those presented in Figure 2:

The most representative flow field patterns:

- **Parallel flow field**: characterized by multiple parallel channels connected by inlet and outlet manifolds located at opposite ends of the plate [21]. Although simple, this design may lead to non-uniform flow distribution, gas accumulation, and the formation of stagnation zones [22,23].
- **Interdigitated flow field**: designed with disconnected inlet and outlet channels, forcing the reactants to pass through the porous electrode [23,24]. This enhances mass transport but results in higher pressure losses [21].
- **Serpentine flow field**: consisting of a continuous channel path that promotes uniform flow distribution and effective removal of gas bubbles [19]. This configuration is widely preferred due to its superior

electrochemical performance and higher achievable current densities compared to other designs [22]. The associated pressure drop induces forced convection through the porous electrode (under-rib convection), improving reactant transport, although excessive pressure losses may arise depending on channel dimensions and assembly conditions [21,23].

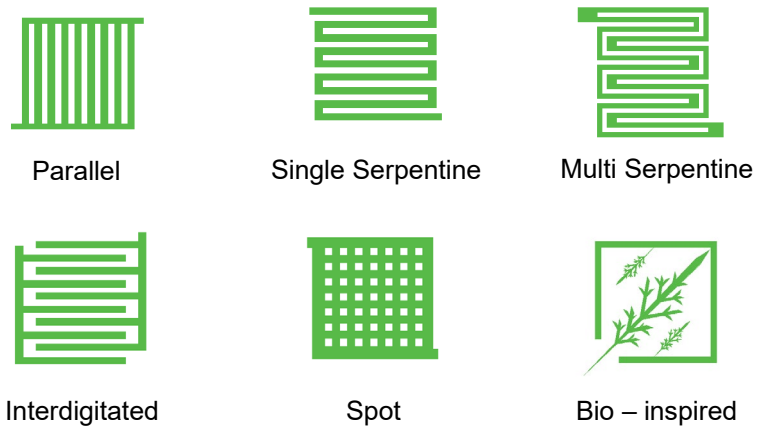

Figure 2. *Representative flow field patterns: parallel, single- and multi- serpentine, interdigitated, spot and bio-inspired designs.*

1.4. Additive manufacturing approaches for electrochemical devices

Additive manufacturing (AM), commonly referred to as 3D printing, has emerged as a promising approach for the fabrication of components in electrochemical devices such as electrolyzers, fuel cells, and batteries. Its main advantages include the ability to produce complex geometries with high precision, reduced material consumption, and rapid design iteration. Several AM technologies are available, including binder jetting (BJT), directed energy deposition (DED), fused deposition modeling/fused filament fabrication (FDM/FFF), powder bed fusion (PBF), sheet lamination (SHL), and vat photopolymerization (VPP) [25].

Among these, FDM/FFF has gained particular attention due to its low cost, accessibility, and versatility, making it especially suitable for manufacturing flow field geometries [26]. However, its application in electrochemical systems is constrained by the intrinsic properties of polymeric materials, which lack the electrical conductivity and corrosion resistance required under harsh operating conditions (acidic or alkaline environments).

To overcome these limitations, different strategies have been proposed. One approach involves fully metallic additive manufacturing, such as stainless steel fabrication via selective laser melting, followed by noble metal coatings to enhance conductivity and corrosion resistance [27]. Alternatively, polymer-based AM combined with metallization has been explored. In this approach, thermoplastic substrates (e.g., ABS) are coated with conductive layers, such as Ni or Au deposited via sputtering, enabling their use as current collectors [28].

Despite these advances, several challenges remain insufficiently addressed in literature. In particular, the use of polymer-based bipolar plates introduces critical mechanical and assembly-related constraints. Compared to metallic components, thermoplastics exhibit lower mechanical strength and are more sensitive to clamping pressure, which can lead to deformation, leakage, or structural failure. While standardized assembly protocols and torque specifications are well established for conventional technologies, such guidelines are largely lacking for AEM electrolyzers. This gap limits the reproducibility and scalability of additively manufactured solutions.

Sputtering is a physical vapor deposition technique widely used to provide conductive coatings on polymeric substrates. It enables the formation of thin, uniform films with good adhesion, high electrical conductivity, and corrosion resistance, depending on process parameters such as deposition time and current [28].

1.5. Objectives and scope of this work

In this context, the main objective of this work is to develop a reproducible design and manufacturing methodology for bipolar plates and flow fields in AEM electrolyzers based on additive manufacturing. The proposed approach aims to exploit the advantages of polymer-based 3D printing to reduce component cost and weight, while enabling electrical conductivity through metallization processes such as sputtering. A key contribution of this work is addressing the lack of standardized design and assembly criteria for additively manufactured bipolar plates. To this end, a dedicated experimental test bench for AEM single cells has been designed and implemented, enabling controlled evaluation of assembly parameters, sealing strategies, and mechanical stability. The scope of the study encompasses the definition of design requirements, material

selection, and manufacturing parameters, as well as the experimental validation of the fabricated plates through leak-tightness tests and preliminary electrochemical characterization.

1. Methodology and Design Framework

This section presents the methodology adopted for the design, manufacturing, and assembly of additively manufactured plates. The approach integrates functional requirements with the constraints associated with polymer-based fabrication, design criteria, material selection, printing parameters, and the adopted sealing strategy.

2.1. General design and development workflow

The design process was initiated through a comprehensive literature review addressing key aspects of AEM cell development at laboratory scale, including flow field geometries, channel and rib dimensions, gasket design, additive manufacturing materials, and assembly procedures. This review revealed a significant lack of standardized guidelines, particularly regarding sealing strategies, torque specifications, and optimal plate geometries for AEM electrolyzers. As a result, several design decisions were defined based on engineering criteria, highlighting the need for reproducible methodologies in this field. The main objective was to validate the feasibility of manufacturing bipolar plates from insulating thermoplastics (e.g., ABS) and enabling their use as current collectors through conductive coatings. This approach is supported by previous work demonstrating that gold sputtering can provide sufficient surface conductivity on 3D-printed plates [29]. Based on these premises, the bipolar plates were designed using CAD software, defining flow field geometry, gasket integration, plate dimensions, and assembly features. The resulting designs were subsequently manufactured and experimentally validated.

2.2. Design requirements for AEM bipolar plates

The bipolar plate design followed an iterative process, considering manufacturing constraints, mechanical stability, and operational requirements.

The main design criteria are summarized as follows:

- **Dimensional accuracy**: To compensate for FDM tolerances, peripheral holes were oversized to 7.15 mm (+0.15 mm), ensuring proper alignment during assembly.
- **Flow field design**: A serpentine configuration was selected due to its proven capability for uniform reactant distribution and efficient gas removal. Although associated with higher pressure drops, this geometry minimizes stagnation zones. Inlet and outlet manifolds were designed with a diameter of 2.5 mm to enable M3 threading and integration of standard fittings.
- **Manufacturing constraints**: Plates were printed with 100 % infill to eliminate internal porosity and ensure impermeability. Surface quality was improved through ironing parameter adjustments (flow rate and nozzle speed), providing a smooth substrate that enhances coating adhesion and prevents delamination.
- **Functional requirements**: Electrical conductivity is achieved via gold sputtering, while PLA and ABS provide adequate mechanical resistance and chemical stability in alkaline environments. The combination of high infill density and improved surface quality ensures both structural integrity and sealing performance.

2.3. Definition of the flow field geometry and design criteria

A single serpentine flow field was selected due to its widespread use and proven performance in electrochemical systems, particularly in terms of uniform reactant distribution and efficient gas removal [19,30–32]. The design consists of 13 serpentine channels across a 25 mm active length, with channel and rib dimensions of 1 mm width and 1 mm depth. These values were chosen based on typical geometries reported in similar-scale cells, aiming to achieve a high open ratio (channel area to total active area relation) while minimizing flow maldistribution [21].

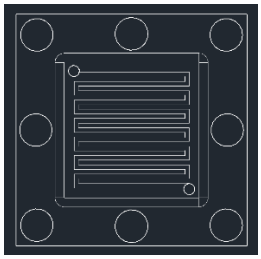

Figure 3. *Schematic of the designed anion exchange membrane electrolyzer plates and flow field geometry.*

The designed plate presented in Figure 3 features external dimensions of 50 x 50 mm^2, a thickness of 5 mm, and an active area of 5 cm^2. Eight peripheral holes were included for clamping, and integrated grooves were designed to accommodate custom gaskets. Fluid distribution is ensured through two 2.5 mm diameter inlet and outlet manifolds. Due to the lack of commercially available O-rings compatible with the plate geometry, and to avoid weak sealing points associated with silicone beads, a custom gasket solution based on injection molding was developed.

2.4. Material selection and additive manufacturing process

The fabrication of bipolar plates by additive manufacturing is a critical aspect of the proposed methodology. Material selection was driven by the alkaline operating conditions of AEM electrolyzers, which demand chemical resistance, impermeability, and sufficient mechanical strength [20]. Thermoplastics such as ABS and PLA were selected due to their processability and compatibility with post-processing techniques. ABS offers superior mechanical strength and chemical resistance, while PLA provides good tensile strength and ductility in addition to the basic characteristics of biodegradable plastics [33].

The plates were manufactured using FDM/FFF technology (Bambu Lab X1 Carbon, 0.4 mm nozzle). CAD designs were generated in AutoCAD and processed in slicing software prior to printing. Surface quality was improved through ironing parameter adjustments (see Figure 4a), with optimal PLA settings identified at 30 % flow and 30 mm/s printing speed.

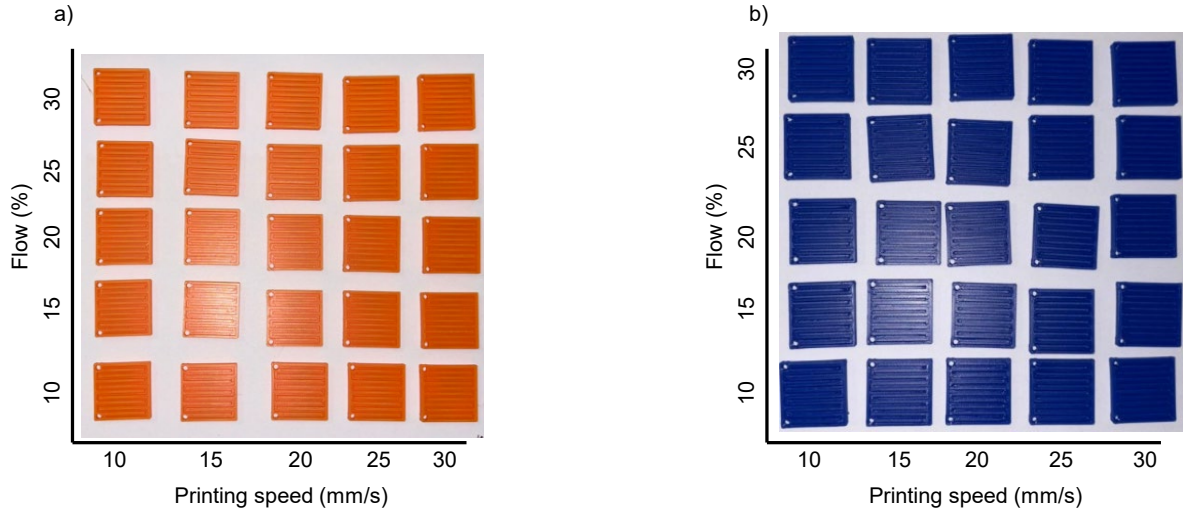

Figure 4. *Surface quality improvement through ironing tests for a) PLA and b) ABS samples.*

2. Experimental Setup

A dedicated experimental protocol was developed to ensure reproducibility in assembly and testing. The methodology includes controlled preparation of samples, definition of assembly procedures, and validation of mechanical integrity prior to electrochemical testing.

3.1. Assembly protocol and reproducibility strategy

Custom gaskets were fabricated using a 3D-printed mold system presented in Figure 5, designed to match the groove geometry of the bipolar plates. A 0.1 mm silicone sheet was used as a release layer to ensure proper demolding and surface finish. The elastomer (Nural 90) was injected into the mold and cured for 24 h.

Figure 5. *Mold used for custom gasket fabrication.*

Prior to assembly, the plates were cleaned with distilled water to remove residual particles. Fluid connections were prepared by machining M3 threads into 2.5 mm printed holes to ensure leak-tight fitting installation. The cell was assembled following a controlled sequence: plates, custom gasket, electrode, and membrane.

Clamping was performed using bolts and spacers, with final tightening applied using a torque wrench at 1.25 N·m in a star pattern to ensure uniform pressure distribution and prevent deformation.

3.2. Gold sputtering process for bipolar plate coating

As polymeric substrates are electrically insulating, conductive coating was applied using gold sputtering. Gold was selected due to its high electrical conductivity and chemical stability under both acidic and alkaline conditions [34]. The metallization protocol was designed to ensure that the flow channels, which feature a deep and narrow geometry (1 mm x 1 mm), were completely coated. The printed plates were cleaned with water and dried using compressed air to remove any dust particles or debris from the printing process. To ensure uniform coating of the 1 mm × 1 mm channel geometry, plates were positioned at an inclination during deposition. The process was performed in 60 s cycles at 50 mA, with intermediate 90° rotations to promote homogeneous coverage. The plates were subsequently flipped to coat both sides, ensuring continuity of the conductive layer across all functional surfaces.

3.3. Description of the AEM single cell test bench

A dedicated test bench (see Figure 6) was developed to evaluate the performance and reproducibility of the AEM single cell system.

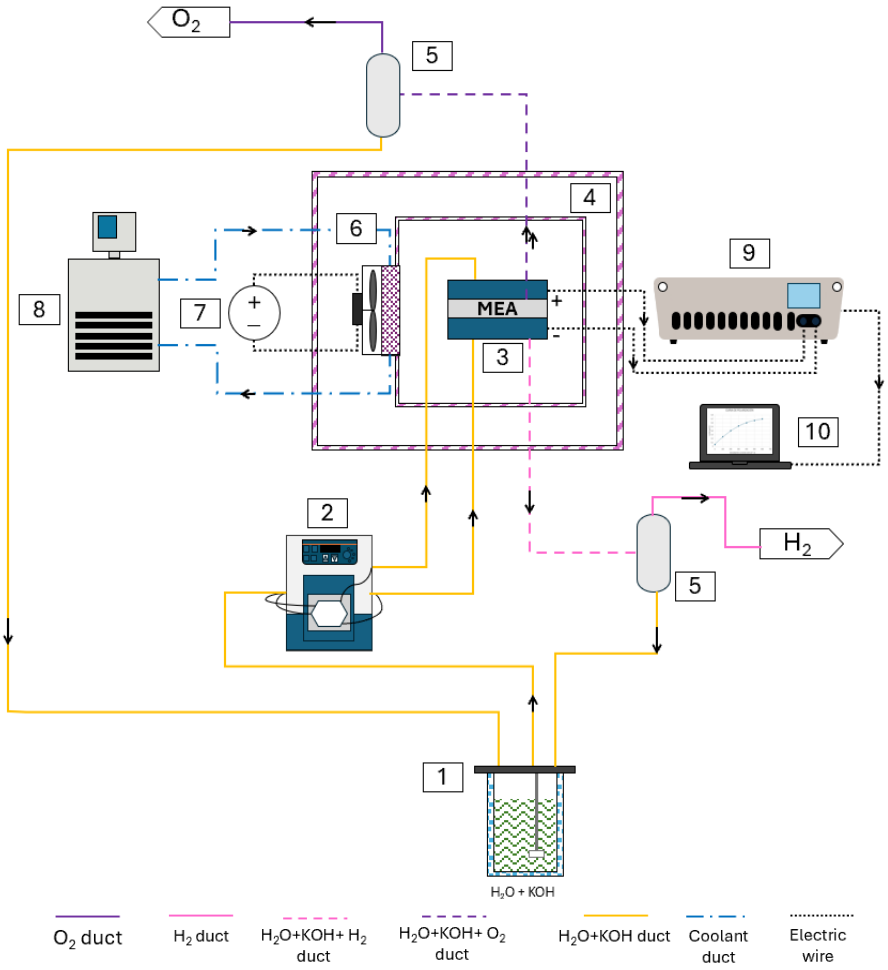

Figure 6. *Diagram of the anion exchange membrane electrolysis test bench. 1-Reactant tank. 2-Peristaltic pump. 3- Single cell. 4- Climatic chambers. 5- Gas-liquid separator. 6- Heat exchanger. 7-DC power source. 8- Refrigerating and heating circulator. 9-Potentionstat-galvanostat. 10-Computer.*

3.4. Leak tightness and mechanical stability assessment

Leak-tightness tests (se test configuration in Figure 7) were conducted to validate the sealing performance and mechanical integrity of the fabricated plates. These tests were performed without electrodes or membrane to isolate the sealing behavior of the assembly. The cell was assembled using PLA plates, custom-made Nural 90 O-rings (fitted with a 0.1 mm silicone sheet acting as a dummy membrane and electrode), 7 mm bolts with their respective nuts, spacers, and inlet/outlet fittings for the manifolds. A controlled tightening protocol was applied using a torque wrench at 1.25 N·m in a star pattern to prevent deformation.

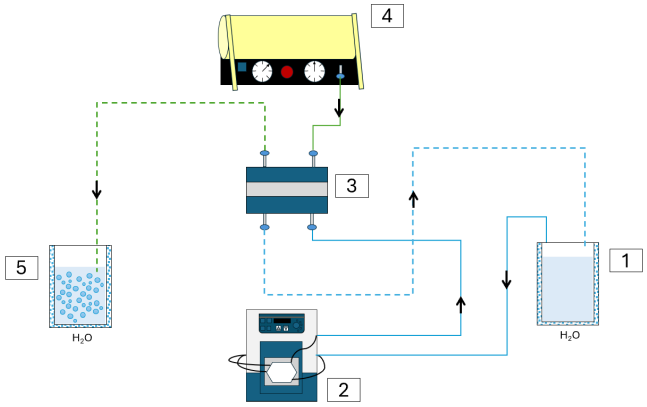

Figure 7. *Diagram of the leak-tightness test configuration for water and air. 1-Aqueous tank. 2-Peristaltic pump. 3- Single cell. 4- Air compressor. 5- Liquid and bubble observation tank.*

4. Results and Discussion

The following section presents the results of the evaluations carried out on the coating of the bipolar plates via sputtering, as well as the leak and mechanical stability tests, analyzing the reproducibility and integrity of the assembled system.

4.1. Manufacturing results and plate integrity

The improvement of additive manufacturing parameters enabled the production of bipolar plates with good surface quality and dimensional accuracy. For PLA, best ironing conditions (30 % flow, 30 mm/s) resulted in smooth surfaces and well-defined channels, while ABS required lower printing speeds (30 % flow and 20 mm/s) to ensure adequate layer adhesion. Dimensional tolerances were validated during assembly, with oversized holes (7.15 mm) enabling proper alignment of bolts and spacers. Custom gaskets fabricated via injection molding (see Figure 8) exhibited uniform geometry and good adaptability to the plate grooves, ensuring effective sealing.

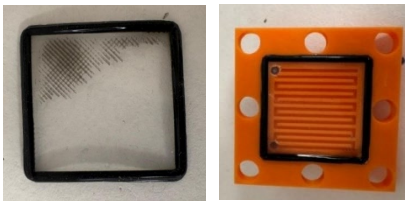

Figure 8. *Fabricated gasket and integration into the plate.*

The assembly procedure demonstrated good reproducibility. Components remained properly aligned within the active area, and no deformation or cracking was observed after applying the defined torque. Uniform compression of the cell confirmed the mechanical stability of the design.

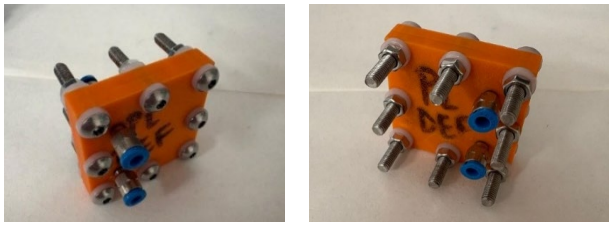

Figure 9. *Assembled anion exchange membrane electrolyzer single cell.*

Following full assembly (see Figure 9), a preliminary leak test was conducted by pressurizing the cell with water. To further ensure hermetic integrity, the cell was submerged in a water bath and subjected to high-flow air and water rates. Leak tests confirmed the integrity of the system. No bubble formation was observed under water immersion or during high-flow air and water tests, indicating a fully sealed assembly. These results validate the proposed sealing strategy and assembly protocol.

After the sputtering process, a uniform and continuous gold layer was observed on the ABS plates, both on flat surfaces and within the flow channels. This confirms that the selected sputtering parameters (50 mA, 60 s cycles) enable adequate coating penetration in high-aspect-ratio geometries, providing electrical conductivity

suitable for use as current collectors. Figure 10 shows the before and after with a thin gold layer of micrometer thickness.

a) b)

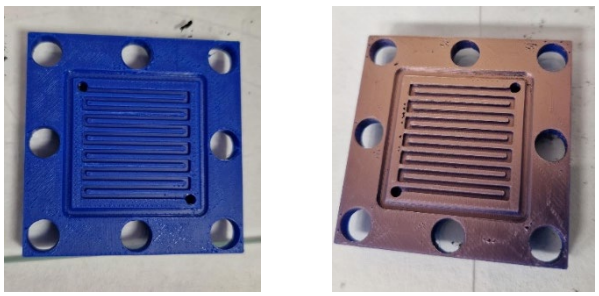

Figure 10. *ABS plate a) before and b) after gold sputtering.*

5. Conclusions and future work

This study demonstrates the feasibility of manufacturing functional bipolar plates using polymer-based additive manufacturing combined with conductive coatings. The optimized design, printing parameters, and controlled assembly procedure result in a mechanically stable and reproducible cell with reliable sealing performance. A key contribution of this work is the establishment of a practical methodology for the fabrication and assembly of additively manufactured bipolar plates, addressing the current lack of standardized procedures in AEM electrolyzers. Future work will focus on electrochemical characterization under real operating conditions, including polarization curves, current density evaluation, and long-term stability testing, to assess the performance and durability of the proposed system.

Acknowledgements

This work was funded by the Community of Madrid through the R&D Activities Program in Technologies (2024), via the project SOLENER-CM, Ref. TEC-2024/ECO-31, under ORDER 5696/2024, dated December 10th (B.O.C.M. No. 307, pp. 108–129). This work was also funded by the European Union's Horizon Europe research and innovation programme under the POSEIDON project (POwer StoragE In D OceaN), Grant Agreement No. 101096457, funded under call HORIZON-CL5-2022-D5-01-02 – Innovative energy storage systems on-board vessels.

References

[1] I. Elegbeleye, O. Oguntona, and F. Elegbeleye, "Green hydrogen production via electrolysis: Materials innovation, system integration, and global deployment pathways," Renewable and Sustainable Energy Reviews, vol. 229, no. 2, p. 116617, Apr. 2026, doi: 10.3390/hydrogen6020029.

[2] W. Aboueata, U. Hijawi, A. Al-Kababji, A. Mohieddine, and P. Choe, "Statistical Analysis of Renewable and Non-renewable Energy Consumption against Population Growth," IOP Conf. Ser. Earth Environ. Sci., vol. 726, no. 1, p. 012003, Apr. 2021, doi: 10.1088/1755-1315/726/1/012003.

[3] Y. G. Cuellar Pérez, J. R. Bermúdez Santaella, and D. A. Herrea Susa, "Hidrógeno verde revisión del estado del arte de las tecnologías de generación para la descarbonización del sector energético," Ingeniería y Competitividad, vol. 26, no. 3, Aug. 2024, doi: 10.25100/iyc.v26i3.14190.

[4] M. E. Şahin, "An Overview of Different Water Electrolyzer Types for Hydrogen Production," Energies (Basel)., vol. 17, no. 19, p. 4944, Oct. 2024, doi: 10.3390/en17194944.

[5] F. Mustapha, D. Guilbert, and B. Gross, "Advancements in anion exchange membrane electrolysers: from catalysts to life cycle assessment," International Journal of Sustainable Energy, vol. 44, no. 1, Dec. 2025, doi: 10.1080/14786451.2025.2520812.

[6] M. Muhyuddin et al., "Anion-Exchange-Membrane Electrolysis with Alkali-Free Water Feed," Chem. Rev., vol. 125, no. 15, pp. 6906–6976, Aug. 2025, doi: 10.1021/acs.chemrev.4c00466.

[7] S. Sebbahi et al., "A comprehensive review of recent advances in alkaline water electrolysis for hydrogen production," Int. J. Hydrogen Energy, vol. 82, pp. 583–599, Sep. 2024, doi: 10.1016/j.ijhydene.2024.07.428.

[8] C. Liu et al., “Development of advanced anion exchange membrane from the view of the performance of water electrolysis cell,” Journal of Energy Chemistry, vol. 90, pp. 348–369, Mar. 2024, doi: 10.1016/j.jechem.2023.11.026.

[9] D. G. Caglayan et al., “Low-cost, high-performance electrodes for PGM-free AEM water electrolyzers: Structural optimization of NiMo-based cathodes,” Applied Catalysis B: Environment and Energy, vol. 378, no. 11, p. 125558, Dec. 2025, doi: 10.1016/j.ijhydene.2019.12.161.

[10] S. Bashiri, M. Amirsalehi, and W. E. Mustain, “Enhancing the Durability of AEM Water Electrolyzers with Aemion Polymers and PGM-Free Anodes,” ECS Meeting Abstracts, vol. MA2025-02, no. 40, pp. 1931–1931, Nov. 2025, doi: 10.1149/MA2025-02401931mtgabs.

[11] C. Li and J.-B. Baek, “The promise of hydrogen production from alkaline anion exchange membrane electrolyzers,” Nano Energy, vol. 87, p. 106162, Sep. 2021, doi: 10.1016/j.nanoen.2021.106162.

[12] L. Yang et al., “Membrane Electrode Assembly Design for High-Efficiency Anion Exchange Membrane Water Electrolysis,” Research, vol. 8, Jan. 2025, doi: 10.34133/research.0907.

[13] J. Gao et al., “Recent advances in anion exchange membranes,” Chinese Journal of Structural Chemistry, vol. 44, no. 5, p. 100563, May 2025, doi: 10.1016/j.cjsc.2025.100563.

[14] L. Titheridge, S. K. Sharma, A. Soisson, C. Roth, and A. T. Marshall, “Recent advances in understanding catalyst coated membranes vs catalyst coated substrates for AEM electrolysers,” Feb. 01, 2025, Elsevier B.V. doi: 10.1016/j.coelec.2024.101607.

[15] W. U. Mulk et al., “Electrochemical hydrogen production through anion exchange membrane water electrolysis (AEMWE): Recent progress and associated challenges in hydrogen production,” Int. J. Hydrogen Energy, vol. 94, pp. 1174–1211, Dec. 2024, doi: 10.1016/j.jcou.2023.102555.

[16] E. Antolini, “Iridium As Catalyst and Cocatalyst for Oxygen Evolution/Reduction in Acidic Polymer Electrolyte Membrane Electrolyzers and Fuel Cells,” ACS Catal., vol. 4, no. 5, pp. 1426–1440, May 2014, doi: 10.1021/cs4011875.

[17] N. Du, C. Roy, R. Peach, M. Turnbull, S. Thiele, and C. Bock, “Anion-Exchange Membrane Water Electrolyzers,” Chem. Rev., vol. 122, no. 13, pp. 11830–11895, Jul. 2022, doi: 10.1021/acs.chemrev.1c00854.

[18] N. Carboni, M. A. Navarra, S. Passerini, and J. Garche, “Durability and degradation of Anion Exchange Membranes in water electrolyzers,” J. Mater. Chem. A Mater., 2026, doi: 10.1039/D5TA06423F.

[19] X. LI and I. SABIR, “Review of bipolar plates in PEM fuel cells: Flow-field designs,” Int. J. Hydrogen Energy, vol. 30, no. 4, pp. 359–371, Mar. 2005, doi: 10.1016/j.ijhydene.2004.09.019.

[20] S. Zhang, H. Xu, Z. Qu, S. Liu, and F. K. Talkhoncheh, “Bio-inspired flow channel designs for proton exchange membrane fuel cells: A review,” J. Power Sources, vol. 522, p. 231003, Feb. 2022, doi: 10.1016/j.jpowsour.2022.231003.

[21] V. L. Meca. “Methanol electrolyser and direct methanol fuel cell for marine applications,” Universidad Politécnica de Madrid, 2024. doi: 10.20868/UPM.thesis.82633.

[22] Y. Wang et al., “Materials and flow fields of bipolar plates in polymer electrolyte membrane water electrolysis: A review,” Energy Reviews, vol. 4, no. 2, p. 100132, Jun. 2025, doi: 10.1016/j.enrev.2025.100132.

[23] Z. Duan, Z. Qu, Q. Ren, and J. Zhang, “Review of Bipolar Plate in Redox Flow Batteries: Materials, Structures, and Manufacturing,” Electrochemical Energy Reviews, vol. 4, no. 4, pp. 718–756, Dec. 2021, doi: 10.1007/s41918-021-00108-4.

[24] S. Karimi, N. Fraser, B. Roberts, and F. R. Foulkes, “A review of metallic bipolar plates for proton exchange membrane fuel cells: Materials and fabrication methods,” Advances in Materials Science and Engineering, vol. 2012, 2012, doi: 10.1155/2012/828070.

[25] M. Koltsaki and M. Mavri, “A Comprehensive Overview of Additive Manufacturing Processes Through a Time-Based Classification Model,” 3D Print. Addit. Manuf., vol. 11, no. 1, pp. 363–382, Feb. 2024, doi: 10.1089/3dp.2022.0167.

[26] L. R. G. Silva, C. E. C. Lopes, A. A. Tanaka, L. M. F. Dantas, I. S. Silva, and J. S. Stefano, “Electrochemical Biosensors 3D Printed by Fused Deposition Modeling: Actualities, Trends, and Challenges,” Biosensors (Basel)., vol. 15, no. 1, p. 57, Jan. 2025, doi: 10.3390/bios15010057.

[27] D. Kim et al., “Three-Dimensionally Printed Metal-Coated Flow-Field Plate for Lightweight Polymer Electrolyte Membrane Fuel Cells,” Energies (Basel)., vol. 18, no. 6, p. 1533, Mar. 2025, doi: 10.3390/en18061533.

[28] M. Amer and A. J. Ghazai, “Effect of Films Thickness on Structural and Optical Properties of Gold (Au) Thin Films Prepared by DC Magnetron Sputtering,” Iraqi Journal of Science, pp. 1549–1556, Apr. 2022, doi: 10.24996/ijs.2022.63.4.15.

[29] Ó. Santiago Carretero, “Direct methanol fuel cell stacks optimization and improvement of components for engineering applications: a design approach,” Universidad Politécnica de Madrid, 2021. doi: 10.20868/UPM.thesis.68984.

[30] R. Ahmed et al., “Bipolar plate flow channel designs for vanadium redox flow battery: a review,” J. Power Sources, vol. 665, p. 239101, Feb. 2026, doi: 10.1016/J.JPOWSOUR.2025.239101.

[31] X. Li, “Bipolar plates and flow field design,” Fuel Cells for Transportation: Fundamental Principles and Applications, pp. 305–337, Jan. 2023, doi: 10.1016/B978-0-323-99485-9.00003-4.

[32] Y. Wang et al., “Review of Flow Field Designs for Polymer Electrolyte Membrane Fuel Cells,” Energies (Basel)., vol. 16, no. 10, p. 4207, May 2023, doi: 10.3390/en16104207.

[33] M. R. Khosravani, J. Schüürmann, F. Berto, and T. Reinicke, “On the Post-Processing of 3D-Printed ABS Parts,” Polymers (Basel)., vol. 13, no. 10, p. 1559, May 2021, doi: 10.3390/polym13101559.

[34] G.-E. Jang and G.-Y. Cho, “Effects of Ag Current Collecting Layer Fabricated by Sputter for 3D-Printed Polymer Bipolar Plate of Ultra-Light Polymer Electrolyte Membrane Fuel Cells,” Sustainability, vol. 14, no. 5, p. 2997, Mar. 2022, doi: 10.3390/su14052997.